

Using Elastic Energy Considerations to Explain Rafting in Ni-based Superalloys With A High γ' Volume Fraction

Catherine Marion Cress

A Dissertation submitted to the Faculty of Science,
University of the Witwatersrand, Johannesburg,
for the Degree of Master of Science

Johannesburg 1993

Abstract

A simple three-dimensional model of a high γ' volume fraction Ni-based alloy is developed. The model is based on the idea that a unit volume in the superalloy can be represented by a cuboidal precipitate with thin 'slabs' of matrix material 'stuck' onto its faces in such a way that coherency is maintained. Rafting is investigated by considering the changes in total energy when the cuboidal precipitates start to flatten into plate shapes or lengthen into rod shapes. It is assumed that inelastic effects are negligible.

Internal and external stresses and strains are determined. Expressions for the derivative of the total energy with respect to a shape parameter are then calculated in the absence of applied stress and in the presence of applied stress. Predictions of rafting behaviour are made for six alloys. Excellent agreement is found with experimental evidence but it is suggested that the agreement is fortuitous.

Acknowledgements

I would like to thank the following people for their contributions to this dissertation:

- Prof. Nabarro, for being such an excellent teacher.
- Rob, Rob. MBS and the people in the NMR lab for the loan of their computer equipment
- Hilton and the Family for all the support and encouragement.

List of Tables and Figures

Table

- I.1 Summary of rafting behaviour observed
- I.2 Predictions made by Pineau's model
- III.1 Calculated values of internal stresses compared with those obtained in FE analyses
- III.2 Data used to obtain results in Table III.3
- III.3 Results of substitution into equations 1 and 2

Figure

- I.1 Pollock and Argon's outline of kinetics
- II.1 Schematic diagram of alloy
- II.2 The unit volume considered in this model
- II.3 The assembly of slabs and cube to form the configuration observed
- II.4 Changes in the unconstrained slab and cube dimensions when rafting occurs
- II.5 Assembled state of slabs and cube
- II.6 Rafting under applied stress - disassembled and assembled configurations
- IV.1 Strains resulting from applied stress

Table of Contents

Chapter	Page
I. Background Study	
I.1 Historical Perspective.....	1
I.2 Observations of Rafting.....	2
I.3 Models of Rafting.....	10
I.4 The Purpose of This Study.....	17
II. A New Model for Rafting	
II.1 Outline of Model.....	18
II.2 Elastic Stability Analysis in the Absence of Applied Stress.....	20
II.3 Stability analysis in the Presence of Applied Stress.....	24
III. Results	
III.1 Internal Stresses Calculation.....	28
III.2 Internal Energy Calculation.....	29
III.3 Calculation of Elastic Energy Changes in the Presence of Applied Stress.....	29
IV. Discussion	
IV.1 The Internal Energy Result.....	31
IV.2 Interpretation of the Full Applied Stress Result.....	32
IV.3 The Approximation $m=n$	33
IV.4 Unreliable Elastic Constants.....	35
IV.5 Reconsidering the Problem.....	36
IV.6 Comparing the Model with Applied Stress Observations.....	36

Chapter I

Background Study

I.1 Historical Perspective

The history of superalloys strictly dates back to around 7000 B.C. when people first began to make objects from copper as opposed to stone. It took about another 4000 years for the benefits of alloying to be realised when it was discovered that copper could be cast more easily if tin or arsenic were added to it. A more important result of these additions was the solid solution strengthening that made bronze a better material for use in tools and weapons. Since the onset of the Bronze Age the ever increasing demand for better tools and weapons has driven the metals industry to more sophisticated technologies.

The jet engine 'revolution' of the 1930's was, initially, the driving force behind the development of the superalloy. It required materials that could be used at the extremely high temperatures and under the severe stresses encountered in gas turbine engines.

Around 1930 experiments were done with small amounts of titanium and aluminium added to the then well known '80/20' nickel-chrome alloy. Significant creep strengthening was found. Further research showed that these nickel-based so-called 'superalloys' with their close-packed FCC crystal structure could have the properties required for use in jet engines. Cobalt- and iron-based superalloys also showed promise in similar applications.

By the 1940's an important aspect of the strength of the nickel-based superalloys had been identified: fine coherent precipitates with an ordered crystal structure were observed embedded within the disordered solid solution matrix. The precipitate phase became known as the γ' phase and the matrix as the γ phase. Observations of γ' revealed that it can be widely alloyed, its yield strength increases with temperature and it has good oxidation resistance, making it a very useful strengthener.

In the 50's and 60's much experimentation was done on improving the properties of the superalloys by changing their chemical composition.

- Aluminium was identified as the primary γ' former and as an important protective oxide forming element, Al_2O_3 scales forming on surfaces at high temperatures.
- Titanium and niobium were also added for their γ' forming capabilities.
- Solid solution strengthening of the matrix was developed through additions of cobalt, molybdenum and other refractory elements e.g. tungsten and later hafnium. These elements were also combined with carbon to strengthen grain boundaries.

- Chromium was always present to improve oxidation resistance; attempts to reduce the Cr content so as to improve strength properties led to hot corrosion problems.
- It was found that careful control of chemical composition could also prevent the formation of undesirable phases - such as σ , μ and Laves phases - which invariably degraded the properties of the superalloy.

After the 60's the chemical composition of nickel-based superalloys varied relatively little but much work was done on the processing of the superalloys. The advent of vacuum melting around 1950 had allowed major improvements in the processing of superalloys but it was in the 70's and 80's that process development really became important. This ultimately led to directionally solidified and single crystal alloys.

Today, over 50% of an advanced jet aircraft engine is made of nickel-based superalloys and the aerospace industry continues to drive advances in the field. However, superalloys also see service in industrial gas turbines, space vehicles, rocket engines, nuclear reactors, submarines, petrochemical equipment and in other machinery that requires long-term strength and corrosion resistance at high temperatures.

I.2 Observations of Rafting

A modern nickel-based superalloy, after complete ageing, consists of a periodic array of cuboidal γ' precipitates aligned along $\langle 100 \rangle$ directions. The coherent precipitates are typically $0.2-0.5\mu\text{m}$ in length and make up about 60% of the volume fraction of the superalloy. A 'misfit' parameter is defined to describe the difference in unconstrained lattice parameters of γ' and γ :

$$\delta = 2 \frac{a' - a}{a' + a}$$

Usually, $|\delta| < 0.005$ and is temperature dependent as a result of differing thermal expansion coefficients in the two phases.

The term 'rafting' refers to the changes in morphology of the precipitates at high temperatures - certainly above 750°C , but often even higher temperatures are required. At these temperatures γ' cuboids link together to form 'rafts'. Rafting has been observed in the absence of an applied stress. In this case the rafts are randomly orientated on $\{100\}$ planes. More commonly observed, is a directional evolution of morphology in the presence of a uniaxial stress. In this case two types of behaviour are observed:

- 'N' type behaviour when the cuboids coarsen normal to the applied stress to form plates
- 'P' type behaviour when the cuboids coarsen parallel to the applied stress to form rods or in some cases plates which lie parallel to the stress direction.

The Effects of Rafting on Mechanical Properties

Rafting has a significant effect on the mechanical properties of Ni-based superalloys. When a rafted morphology was compared with cuboidal precipitates, negative effects [36,45] and positive effects [14,30] were reported. In 1986 the apparently conflicting observations were rationalised by Caron et al [85]. They suggested:

- At low temperatures and high stresses, rafting degrades the creep properties. Under these conditions the dominant creep mechanism is the shearing of γ' particles with γ/γ' interfaces as barriers to the process. Rafting decreases the surface area of these barriers and thus allows more γ' shearing.
- At high temperatures and low stresses rafting improves the performance of the alloy. Under these conditions the dominant creep mechanism is climb of dislocations over γ' particles and rafts provide longer climb paths than cuboids.

When rafted morphologies were compared with each other, it was found that more perfectly lamellar rafts were more desirable than irregular rafts [32,42].

It is clear that understanding the processes involved in rafting is important for the designers and the users of Ni-based superalloys. It has thus been the subject of a great deal of research over the past 27 years.

Observations of Rafting in the Absence of Applied Stress

A study of the modulated structure of Ni-Al alloys was done by Ardell and Nicholson [9] in 1966. They investigated the ageing of a Ni-6.7wt%Al alloy at 750°C and 775°C. Observations were made of spherical precipitates that were randomly distributed evolving into larger cuboidal precipitates that were aligned along $\langle 100 \rangle$ directions. Upon further ageing the particles either coalesced or coarsened into plates on {100} planes. They pointed out that elastic interactions between precipitates could explain the alignment process.

Ardell and Nicholson's observations were important in that it was seen that precipitates could move from a cuboidal shape to a plate shape by coalescence, i.e. raft, even when no stress was applied. Similar observations were reported by Miyazaki et al [20], Sadiq and West [79] and Nathal [42]. The plates observed in [42] - and those observed in Nathal and Ebert's earlier study [40] - were fairly irregular. In both [40] and [42] some loss of coherency was reported.

Observations of Rafting Under Applied Stress

In the 50's and early 60's there were comments on the 'modulation' of the γ' precipitates in nickel-based superalloys but apparently no discussions of the rafting phenomenon. Towards the end of the 60's observations of rafting in Ni-based alloys were recorded during creep

tests [4-8]. Some dependence on direction of applied stress was apparent but was not discussed in detail.

A summary of the rafting directions observed for various materials and test conditions from 1970 onwards is given in Table I.1.

Table I.1 Summary of rafting behaviour observed

Authors (Ref) year	Alloy	Misfit given	Misfit corrected*	Elastic constants (GPa)	Test Conditions	γ' vol frac.	Rafting Obs'd	
							Tens.	Comp.
Tien & Copley [12,13] '71	Udimet 700	+0.02%	-0.3%[49]	$\gamma' \sim 10\%$ softer	950°C 147 MPa	0.35	N	P
Carry & Strudel [16] '78	Alloy 01	-0.4%	0.38%[17]	-	750°C-950°C 190 MPa-300 MPa	0.38-0.61	P	
Miyazaki et al [20] '79	Ni-15at%Al	+0.56%	+0.56%	$C_{11}=112$ $C_{12}=63$ $C_{11}'=167$ $C_{12}'=187$	750°C 147 MPa	~ 0.27	P	N
Pearson et al [30] '80	Alloy 143	-0.78%	-0.82%[44]	-	1038°C 207 MPa	~ 0.6	N	
Caron & Kahn [32] '83	CMSX-2	+0.14%	-0.33%[17]	[52] $C_{11}=109$ $C_{12}=59$ $C_{11}'=125$ $C_{12}'=67$	760°C-1050°C 120 MPa-750 MPa	0.68	N	
Nathal & Ebert [37,38] '83,'85	NASAIR 100	-0.36%	-0.45%[44]	$\gamma' \sim 12\%$ harder [50]	925°C-1000°C a) 148-310 MPa b) $\epsilon=8.4 \cdot 10^7 s^{-1}$	~ 0.6	N	P
MacKay & Ebert [34,35,36] '83,'84,'85	Alloy 143	-0.8%	-0.82%[44]	-	927°C-1038°C 141MPa-234MPa	~ 0.6	N	
Freedholm & Strudel [17,18] '84,'85	Alloy 01	+0.38%	+0.38%	see above	1050°C 140 MPa	~ 0.6	P	
	CMSX-2	-0.33%	-0.33%			0.68	N	
	Alloy 221	-0.23%	-0.23%			0.68	N	
	Alloy 211	$\sim -0.09\%$	$\sim -0.09\%$			0.63	N	
Nathal & Ebert [39,40,42] '84,'85,'87	Alloy C	-0.23%	-0.31%[49]	-	1000°C 148 MPa	0.55	N	
	Alloy E	0.00%	-0.22%[44]			0.57	N	
	Alloy H	-0.17%	-0.17%			0.51	N	
Nathal et al [45] '89	NASAIR 100	-0.4%	-0.4%	$\gamma' \sim 12\%$ harder[59]	760°C 600-690MPa	~ 0.6	N	
Faller-Kniepmeier & Link [26] '89	SRR 99	-0.21%	-0.21%	[54] $C_{11}=187$ $C_{12}=129$ $C_{11}'=205$ $C_{12}'=133$	980°C 170 MPa	0.7	N	
Conley [27] '89	Ni-Al-Mo alloy i	+0.4%	0.39%-0.6%	-	750°C 250MPa	0.12		N
Pollock & Argon [48] '92	CMSX-3	-0.38%	-0.38%	$C_{11}=202$ $C_{12}=139$ $C_{11}'=179$ $C_{12}'=120$	850°C-1060°C 50 MPa-552 MPa	0.7	N	
	PMA			-	1050°C 50 MPa-150 MPa	0.5	P	

* Better estimates of misfits have often been made after observations were initially published

Apart from the dependence of rafting direction on stress orientation and misfit sign that is apparent in Table I.1, many other observations have been made of stress-aged superalloys:

1. General

At sufficiently high temperatures ($> \sim 950^\circ$) rafts are generally observed to start forming during the primary stage of creep [16-18,30,32,34-38]. The rafting rate increases with increasing temperature and applied stress [36,38,48] and also with increasing lattice misfit [27,40,44].

The γ' volume fraction generally stays constant during rafting [36]. It is, of course, temperature dependent [15,40,43].

2. Raft dimensions

When rafts are formed initially, their average thickness is observed to be very close to the thickness of the original γ' precipitate [16,30-38,42]. The average length of rafts appears to increase linearly with time until the material is fully rafted [35]. This increase is initially a result of the lengthening of individual precipitates but is later determined by the number of cuboids that have merged. Thickening of the γ matrix has been noted [18] as has encapsulation of the γ phase by the γ' phase at large creep strains. The raft-shape is stable [30,35-37] although coarsening of the rafts is observed, especially at the onset of tertiary creep [17,37-39,43].

It is easy to understand that the coarsening observed after rafting will degrade the creep properties of the alloy since it leads to a decrease in the number of barriers to dislocation motion - regardless of which creep mechanism is operating.

The coarsening is generally considered to be driven by the well-understood process of surface energy reduction. Perfectly lamellar structures are stabilized against this form of thickening since the radius of curvature of interfaces is essentially infinite and the chemical potential is thus constant. Less perfectly formed lamellae have more curved interfaces and one would expect them to coarsen faster if coarsening is driven by surface energy reduction. This is what is observed [43]. The faster coarsening rate associated with irregular rafts gives an important consequence of the rafting phenomenon and explains the observations [32,42], mentioned earlier, that alloys with irregular rafts have worse creep properties than those with regular rafts.

3. Effects of the size and regularity of the initial microstructure

Nathal [42] found that the most cuboidal, regular precipitates produced the most regular rafts under stress. This was also found by Caron and Kahn [32]. In a study by MacKay and Ebert [35] the alloy that had the most regular precipitates exhibited the best creep properties. They attributed its success to the smaller size of the precipitates although it appears that the smaller precipitates also produced more regular rafts. The size of precipitates can, of course, have

an effect on creep properties in the manner they suggested.

The size and regularity of the precipitates also affects the rafting rate. Caron and Kahn [32] observed that rafting is retarded in alloys with irregular precipitates. MacKay and Ebert's [35] smallest precipitates rafted quickest. It makes sense that a smaller precipitate presents shorter diffusion lengths, but once again the regularity of the precipitates was surely also important.

4. The effects of plastic flow

Observations of rafting are generally accompanied by observations of dislocations bowing out on {111} planes through the narrow γ channels and forming dislocation networks at the γ/γ' interfaces.

Misfit relieving dislocation networks:

During over-ageing, in the absence of applied stress, dislocations forming interfacial networks are observed to be near-edge in character and have Burgers' vectors lying in the plane of the interface [18,19,46]. They are arranged in hexagonal networks on γ/γ' interfaces parallel to {111} planes and in square networks on interfaces parallel to {100} planes. It is clear that this is the dislocation configuration that best relieves the misfit strains present in the alloy. The dislocation spacing is generally inversely proportional to the misfit.

Dislocation networks developed under applied stress:

Under the influence of an applied stress, the formation of interfacial dislocation networks is accelerated; at the onset of steady state creep, stable networks have already been established [46,47]. The networks formed under applied stress have different configurations from those produced entirely by lattice misfit strains. The dislocations initially observed are mixed in character and only partially misfit-relieving [18,46,47]. Later, multiple slip systems are activated which produce dislocations that are more efficient at relieving misfit [46].

Differences between observations in channels normal to applied stress and those parallel to applied stress:

During primary creep, in a negative misfit alloy, the channels parallel to a tensile stress have much of their compressive misfit stress relieved; in the channels normal to the tensile stress, the applied stress and internal stress combine to make large shear stresses. Plastic deformation thus occurs more easily in normal channels; in fact, in the initial stages of creep, dislocations are observed only in the normal channels and not in the parallel channels [17,26,46,47]. The reverse effect is assumed for positive misfit alloys.

Gabb et al [46] suggest that the role of dislocations in rafting is small:

When the effect described above was observed by Gabb et al for their negative misfit alloys, they noted that rafting was occurring when dislocations were observed in the normal channels and not observed in the parallel channels. The absence of dislocations in the channels where coalescence was taking place led them to the conclusion that the role of dislocations in rafting is small. This is supported by Fredholm and Strudel's [17] claim that rafting seemed to "precede dislocation multiplication" in the three alloys they studied.

Gabb et al acknowledged, however, that the formation of dislocation networks was an inseparable part of the rafting process. It was suggested by them and by Fredholm and Strudel [17] that the presence of dislocations might provide diffusion short-circuits and thus result in enhanced coalescence.

Gabb et al also noted that, firstly, the networks are fully formed at the same time as the rafting process is completed -generally at about the onset of secondary creep. Secondly, they noted that the dislocation networks first form on the interfaces which do not appear to advance in the rafting process. Both observations suggested that the networks play a role in stabilizing the microstructure.

It was also pointed out that in MacKay and Ebert's [35] tests an abundance of dislocations at interfaces, prior to creep testing, decreases the rate of directional coarsening. However, the alloy with no dislocations prior to testing was the one that had the most regular and cuboidal precipitates. The effects of the different variables on rafting rate are difficult to distinguish.

Pollock and Argon suggest that creep flow is important in rafting:

In Pollock and Argon's study of CMSX-3 [47,48,87,88] very little rafting was observed below 1000°C. After 48h at 1050°C and 50 MPa rafting was only observed in CMSX-3 in some areas of their samples; it was noted that these regions coincided with regions of significant dislocation densities.

As in studies discussed above, they observed an absence of plastic flow in channels where coalescence occurs (channels parallel to an applied tensile stress). They did not draw the same conclusion from this as Gabb et al. Instead, they commented on the evidence that dislocations are always present when rafting occurs. They pointed out that the dislocations will alter the misfit stresses in the matrix and inferred that it is thus "essential to consider the details of the creep flow process in the formulation of a quantitative model.. " of rafting. It was acknowledged, however, that the initial misfit stresses are clearly important driving forces in the rafting process since the process shows such a strong dependence on misfit sign.

Socrate and Parks [49] agreed with Pollock and Argon: they claimed that "it is of fundamental importance to consider the effects of creep flow..."

Misfit relief during creep:

At temperatures around 1000°C, under stresses of about 140 MPa, alloys with regular precipitates generally raft fairly quickly: fully formed rafts have been observed after 20h in CMSX-2 and NASAIR 100 [32,37], after 18h in NASAIR 100 [37], after 20h in alloy 221 [18] and 5h in alloy 143 at a higher stress of 207 MPa [30]. Observations of CMSX-3 [48] are an exception: a uniform rafted structure was only reported after 64h at a temperature of 1060°C and a stress of 138 MPa.

In [47],[87] and [88], Pollock and Argon discuss creep in CMSX-3 at 800-900°C. They claim that misfit stresses are nearly eliminated by the time steady state creep begins. This is consistent with Gabb et al's observations except that in CMSX-3 the networks are more three dimensional as no rafting has occurred.

For alloy 221 at 1050°C and 140MPa [17,18], the beginnings of rafting were observed 1h into a creep test - less than about one twentieth of the time taken before the onset of secondary creep i.e. less than about one twentieth of the time taken to "nearly relieve the misfit stresses". At such an early stage of creep it seems unlikely that misfit relief could significantly alter the misfit stresses in the material. The alloy in which this was observed had a fully developed rafted structure at 20h. This suggests that in the other alloys mentioned above (excluding CMSX-3) it would be reasonable to assume that rafting had started early in the creep process - before misfit relief could play an important role.

Evidence presented by Schneider and Mughrabi [86] supports this claim. They found, for CMSX-4, that there is a slower build up of misfit relieving dislocations at rafting temperatures than at lower temperatures. Their low temperature test conditions (800°C, 654MPa) are comparable with the conditions in much of Pollock and Argon's work presented in [47] (850°C, 552MPa). It seems possible, then, that even less relief of misfit might have occurred at the onset of rafting - and during rafting - than one would have predicted using results in [47]. The reason suggested for the temperature dependence, is that at higher temperatures, interface dislocations can "move away laterally by a combined glide/climb process".

In Schneider and Mughrabi's study, the increase in creep rate observed immediately after the minimum creep rate was attributed to raft formation. They noted that detectable changes in misfit were only first observed after the minimum creep rate was achieved. They say that rafting occurs in a similar fashion to that observed by Feller-Kniepmeier and Link [26] in SRR 99.

In SRR 99 rafting is observed at the onset of "stage II" creep [26]. If stage II creep is equivalent to steady state creep, this is not consistent with claims by Gabb et al and Pollock and Argon that stable networks are present at this stage. It appears that stage II creep in Feller-Kniepmeier and Link's study corresponds better with Schneider and Mughrabi's rafting stage which occurs *before* their "plateau region". If this is the case then rafting will presumably start just before or about the same time as "detectable changes in misfit occur", as in the CMSX-4 study. It does not seem clear how the rafting rate compares to the misfit relief rate: misfit relief could be fast enough to influence the rafting rate, but seems unlikely to reverse the effects. As is discussed below, Socrate and Parks' study [49] suggests

otherwise.

In CMSX-3 rafting is very slow and considering [47] and [48] it seems that the alloy will undergo significant plastic deformation before rafting is complete. Schneider and Mughrabi's observations [86] suggest that there might not be as much plastic deformation as suggested in [47] but still, the conclusion drawn for other alloys does not necessarily apply for CMSX-3.

5. Observations of element concentration during rafting

Svetlov et al [28] crept samples of SC-83 to rupture at 900°C under a stress of 600 Mpa. They then investigated the concentration of elements in various areas of their samples. The beginnings of N-type rafting were observed: in channels parallel to the applied stress higher concentrations of γ' forming elements (Al, Ta) and lower concentrations of γ elements (Mo, Cr) were found when compared to channels normal to the applied stress.

They explain their observations by suggesting that large atoms, which are also γ' forming elements, move from the less compressed channels to more compressed ones so as to relieve the pressure. However, their rough estimates of stresses in γ' channels seem to indicate that the vertical channels are more compressed than the horizontal ones. This seems to imply the movement of large atoms in the opposite direction to that observed.

Directional Coarsening in other alloys

Directional coarsening of precipitates in alloys that are not nickel-based has also been observed:

- 1 In an Fe-N alloy [59] plate-like precipitates formed on all {100} planes in the absence of applied stress but favoured the plane normal to an applied tensile stress and showed some evidence for precipitation being inhibited normal to a compressive stress.
- 2 Rod-like Pb_3Na precipitates with a negative misfit were observed [60] to coalesce perpendicular to a tensile stress and parallel to a compressive stress.
- 3 Plate-like, Au-rich precipitates in an Fe alloy [61] formed on all {100} planes in the absence of applied stress but normal to an applied tensile stress. The misfit was -0.1% parallel to the plate and 40% normal to it.
- 4 In an Al-Cu [62] alloy plate-like θ' precipitates formed on all {100} planes in the absence of applied stress. Stress applied along [001] favoured precipitation on (100) and (010) in the compressive case and on (001) in the tensile case. The misfit was said to be 1.36% parallel to the plate and -28.2% normal to the plate.
- 5 A similar alloy was studied by Eto and Mori [63] and the reverse effects were observed. No misfit was given.

In cases 1 and 5 the authors claimed that the stress affected precipitation during nucleation and in 3 the author claimed it effected the coarsening phase.

The observations in these alloys show some resemblance to those in the Ni-based alloys in their responses to tensile and compressive stresses and the possible dependence of alignment on misfit. The observations clearly differ in that none of the alloys exhibit a cuboidal stage and the misfit is generally tetragonal. The authors' claim that the applied stress affects the nucleation stage and not the coarsening stage of precipitation also is in disagreement with observations in Ni-based alloys. It seems fairly likely, though, that findings for Ni-based alloys could have application for other alloys with misfitting precipitates.

An Alternative Elastic Energy Effect

In 1957 Westbrook [64] published his observations of what he called octodically diced cubes of Ni₃Al precipitate in Ni-Al alloys. Since then, many observations [65-68] have been made of these collections of eight cubes of precipitate all arranged on a master cube within the matrix. In the same samples one often finds a configuration where two plates of precipitate are arranged on a master cube. The phenomenon is explained [65-67,69-73] and modelled [74,75] using elastic interaction considerations; the theory is based on the idea that the decrease in elastic energy when a cuboidal precipitate breaks up into cubes or plates more than compensates for the increase in interfacial energy.

It appears that the cube splitting phenomenon and the rafting phenomenon can both be observed in a single alloy, e.g. SRR 99 [53] and the Ni-15Al alloys of Miyazaki et al [20,73] but generally observations of cube splitting are limited to Ni-based alloys with large misfit ($|\delta| > \sim 0.5$) and low γ' volume fraction ($f < \sim 0.5$) [73] as opposed to the rafting phenomenon which generally appears in smaller misfit, higher γ' volume fraction alloys.

II.3 Models of Rafting

Tien and Copley

Tien and Copley [12,13] developed a theory of rafting based on minimisation of bulk precipitation strain energy. Using the positive misfit given in their paper, the theory correctly predicted the morphology of precipitates in Udimet 700 after ageing under stress. At high temperatures it appears that Udimet 700 has, in fact, a negative misfit [49]; using the corrected value, the theory does not predict correctly. Problems with the theory are discussed at length by Chang and Allen [24].

Pineau

In 1976 Pineau [21] developed a model based on Eshelby's equivalent inclusion method [22,23]. Assuming the material was isotropic, he was able to compute the total elastic energy of a single ellipsoidal inhomogeneity in an infinite matrix. The result was a map giving the most stable ellipsoidal shape (sphere, oblate ellipsoid or prolate ellipsoid) as a function of the misfit, the applied stress and the ratio of Young's modulus in γ' to that in γ . Spheres were taken as an approximation to cubes, oblate ellipsoids as plates and prolate spheroids as needles.

By estimating a suitable substitute for the ratio of Young's moduli from the information on elastic constants in Table I.1 one can obtain ten data points for Pineau's stability map. The predicted rafting for the ten points is shown in Table I.2 and compared with observed rafting directions.

Unfortunately, most of the data points fall into (denoted '?') or close to (denoted '?X') regions of uncertainty where Pineau's graphical solution technique does not provide a conclusive prediction of preferred shape. The one point that does fall into a clearly defined area does not predict the correct direction of rafting.

Table I.2 Predictions made by Pineau's model

Alloy	σ (MPa)	δ (%)	$\frac{\sigma}{\delta E}$	E'/E	Raft pred.	Raft Obs.
Udimet700	148	-0.3	-0.31	0.9	?N	N
	-148	-0.3	0.31	0.9	N	P
Ni-15Al	147	+0.56	0.39	1.23	?	P
	-147	+0.56	-0.39	1.23	?P	N
NASAIR100	148	-0.45	-0.46	1.12	?N	N
	-148	-0.45	0.46	1.12	?	P
	600	-0.45	-1.85	1.12	?N	N
CMSX-2	140	-0.33	-0.62	1.14	?N	N
CMSX-3	50	-0.38	-0.15	0.92	?N	N
	150	-0.38	-0.4	0.92	?N	N

Obvious problems with Pineau's model are:

- (i) It deals with an isolated inclusion in an infinite matrix and so is inappropriate for most modern superalloys which have high γ' volume fractions

- (ii) It is based on isotropic elasticity when Ni-based alloys are generally highly anisotropic;
- (iii) Ellipsoids are considered in place of the observed parallelepiped shapes
- (iv) It does not take into account the effect of plastic deformation.

Despite the shortcomings of Pineau's model, it gave a very thorough account of morphological evolution, under the influence of a uniaxial stress, in the low γ' volume fraction alloys available in 1976.

Miyazaki et al

In 1979 Miyazaki et al [20] performed similar calculations of strain energies, this time basing them on anisotropic elasticity theory and including interfacial energy considerations. Their model correctly predicted that the precipitates in their alloy would generally exhibit P-type behaviour under tension and N-type behaviour under compression. They also correctly predicted that for their alloy a plate-shaped precipitate was energetically most favourable for all annealing conditions - with plate normals parallel to a compressive stress and perpendicular to a tensile stress.

Using the model they were able to obtain plots of energy vs. aspect ratio and were able to predict more than just the general direction of coalescence. They found:

- (i) In the absence of applied stress, spheres represented a stationary point on the energy vs aspect ratio curve. The point was a minimum for precipitates with radii smaller than 40nm but became a local maximum for larger precipitates. Other shapes were favoured for the larger precipitates.
- (ii) Metastable states were predicted in applied stress cases. They correctly predicted that under tension rods would form during the transitions from cubes to plates. They did not, however predict that rods would form during the transition under compression

The model had shortcomings (i), (iii) and (iv) of the Pineau model. In addition, Miyazaki et al used Lin and Mura's equations [77] for implementation of Eshelby's method; Chang and Allen [24] have shown that these are somewhat unreliable. It not clear whether the model would give qualitatively correct predictions for other alloys.

Chang and Allen

Chang and Allen [24] improved on the model of Miyazaki et al by substituting Asaro and Barnett's [76] equations for Lin and Mura's. The solution method was thoroughly tested using comparisons with analytical solutions for simple cases. To determine the effects of misfit, elastic inhomogeneity and applied stress, 250 combinations of material parameters were investigated.

They claimed that the predicted morphologies are in good agreement with data for CMSX-3 [48], Ni-15Al [20] and Udimet 700 [13]. They have however assumed a positive misfit for Udimet 700; assuming a negative misfit at high temperatures [49], their stability map given does not predict the correct shape. Their map also predicts rod-shaped precipitates for a soft inclusion with negative misfit under tension. CMSX-3 has elastically soft inclusions [48], a negative misfit and plates are observed under tension.

Chang and Allen have neglected to consider interfacial energy. However, Socrate and Parks [49] have pointed out that interfacial energy - and chemical energy - are invariant with respect to the $\langle 100 \rangle$ directions and thus cannot account for the directionality of coarsening. They do, of course, play a fundamental role in the coarsening process. Problems (i), (iii) and (iv) persist and it appears that at least one of these problems prevents correct prediction of rafting direction. It should be noted that if one can neglect interfacial energy then the model used by Miyazaki et al is very similar to Chang and Allen's. Thus, the predictions made by the two models are likely to be the same.

Johnson

Johnson et al [55] developed a model based on a single inhomogeneous ellipsoidal precipitate in an infinite matrix. The sum of the elastic and interfacial energies was expanded into a Taylor series about the spherical precipitate state. Isotropy was assumed for the interfacial energy but not for the elastic energy.

Shapes giving energy extrema were in good agreement with those predicted and observed by Miyazaki et al. Johnson et al, however, gave 125nm - as opposed to the 40nm of Miyazaki et al - as the diameter of precipitate at which, in the absence of applied stress, the sphere no longer represents a minima on the energy vs. shape curve. In both studies the same elastic constants were used but Johnson et al used a larger value for the interfacial energy. The value given by Johnson et al is in agreement with Khachatryan [78]. The effect of metastable states is also discussed.

Once again, the model suffers problems (i), (iii) and (iv). Using a model that starts to eliminate problem (i) Johnson, Abinandanan and Voorhees [56] have studied the coarsening kinetics of two spherical inhomogeneities in an anisotropic matrix under the influence of applied stress. This is still a long way from the system encountered in high γ' volume fraction alloys and the complexity of the formulation makes extrapolations difficult.

Carry & Strudel

In 1978 Carry & Strudel [16] proposed a model for rafting that was based on plastic flow. If they assumed their alloy - alloy 01 - had a negative misfit they could explain the rafting observed. It was later established, however, that the alloy has a positive misfit. Using the corrected value the theory failed to explain the phenomenon.

Pollock & Argon - Finite Element Model

Following the observations described in section 2, Pollock and Argon [48] developed a 2-D model of rafting using finite element analysis. A two dimensional mesh was constructed to give a plane strain approximation to the microstructural geometry of CMSX-3. Principal internal stresses of ~433MPa were calculated in the γ parallel to the phase interfaces and 50 MPa in the γ perpendicular to the phase interfaces. Principal internal stresses in the γ' cuboid were calculated to be 54 MPa.

Initial internal stresses were also calculated for the material when an external stress was applied. The resulting resolved shear stresses on $\{111\} \langle 110 \rangle$ slip systems were determined in the horizontal and vertical matrix channels (with respect to the applied stress). This revealed that stresses in the horizontal channels were bigger than those in the vertical channels by as much as a factor of two. It was pointed out that the reverse would be the case if the applied stress were compressive or if the alloy had a positive misfit. This corresponds well with the observations of dislocation motion discussed in section 1.2: dislocations were initially observed in horizontal channels and not in vertical ones for a negative misfit alloy under tension.

To simulate the effects of an applied stress the γ' was allowed to deform elastically while the γ was allowed to deform elastically and by creep. A simple power law relation was used to describe the creep properties of the matrix

$$\dot{\epsilon}_e = A\sigma_e^n$$

Creep properties for solid solution Ni-6W were used: $n=4.5$, $A=5.4 \times 10^{-15} \text{s}^{-1} \text{MPa}^{-4.5}$. During the primary creep transient most of the misfit stresses were relieved and a plastic strain of 7×10^{-4} accumulated.

As the creep progressed a negative pressure built up in the horizontal channels and a positive pressure in the vertical ones. Since the misfit strains have already been relieved at this stage, this effect would of course not be reversed in the case of positive misfit alloy. The resulting flow of material cannot therefore be the rafting mechanism.

Pollock & Argon - Outline of kinetics

At the end of the paper discussed above, Pollock and Argon outline a possible process for rafting. In their scheme, the precipitate starts to dissolve in regions that are adjacent to the horizontal channels. Subsequent diffusional flow of the γ' forming elements towards the vertical channels and the γ forming elements towards the horizontal channels results in the formation of rafts normal to the stress axis. Dislocations would act as sources and sinks for the vacancies and/or diffusional short-circuits for the process.

Referring to Fig.I.1, one sees that the contraction in γ' size would be:

$$\Delta w = \frac{t}{1+t/w}$$

Assuming a constant γ' volume fraction the precipitates would - in CMSX-3 - ultimately thin by about 10% and the γ thickness would double. Generally rafts are reported to be about the same thickness as the original precipitate but generally not to an accuracy of more than 10%. Some evidence for thinning is, in fact, apparent in [38] and in Nathal's study [43] of the effects of initial size of precipitates on rafting. In four observations in [43], cuboidal precipitates rafted to form lamellae that were thinner by an amount consistent with that given by eq.1.2. Thickening of γ lamellae is also observed [18]. Thus it would appear that the outline given here is consistent with observations.

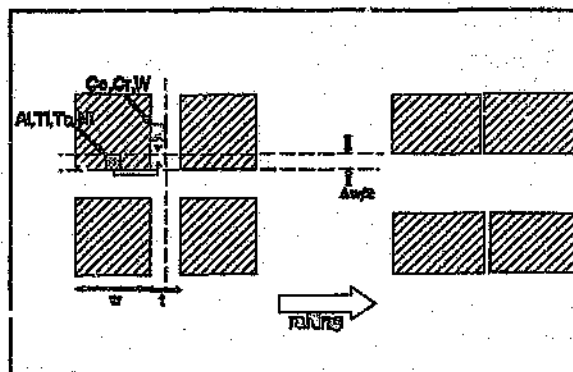


Fig.1.1 Pollock and Argon's Outline of Kinetics

They also showed that using an effective diffusion coefficient calculated from diffusional rounding of cube edges and an average transport distance of a cube length, a characteristic time for initiation of rafting was about 5 hours which is consistent with the observed times.

Socrate and Parks

Socrate and Parks [49] have developed a method of evaluating the generalised force acting on all points of the γ/γ' interface. The force, which is derived from Eshelby's energy momentum tensor is work-conjugate with the normal displacement of the interface. It is thus related to the tendency of the interface to migrate. It is evaluated for a 2-D model using plane strain finite elements to give predictions of rafting behaviour.

Using a purely elastic analysis they obtain results that are consistent with Pineau's stability map, although there is no obvious reason why their results for strongly interacting particles should agree with Pineau's predictions for an isolated inclusion. Their predictions of directions of coarsening are correct for only two of their six sets of data. They conclude from this that purely elastic considerations are not sufficient to predict coarsening directions in nickel based alloys. They go on to do analysis for a system in which the γ matrix can deform elastically and by creep, while the γ' cuboid can only deform elastically. The isotropic power law used is the same as that used by Pollock and Argon - shown above.

Once the matrix is allowed to creep, correct predictions of the direction of coarsening for their data are obtained. The alloys for which incorrect predictions were made using the purely elastic analysis, show no tendency at all to raft under purely elastic stresses which seems strange when one considers the observations discussed in II.2.

Their model has none of the four problems described above for Pineau's model. The purely elastic analysis suffered none of problems (i) to (iii) and it would appear that consideration of inelastic effects is necessary for correct predictions of rafting phenomenon.

But then it is important to remember that Socrate and Parks' model is a 2-D model. It is not

clear what predictions a purely elastic 3-D model appropriate to a high γ' volume fraction alloy might provide. Considering the results for CMSX-3 discussed above, it seems fairly possible that, for this alloy, even a 3-D model would not provide reliable predictions. Nevertheless, a better understanding of the physical processes at work in the purely elastic case could well improve the models that deal with more complicated effects.

Being a 2-D model, Socrate and Parks' model can also provide no information on the problem of rafting in the absence of stress since in 2-D 'flattening' into a plate is equivalent to 'lengthening' into rod just rotated by 90° . Rotation by 90° is a symmetry operation of the crystal in the absence of stress. The difference in energy of these two morphologies is thus zero. This does not hold in the 3-D case: a 3-D rod is not a 3-D plate turned through 90° .

Gayda, Srolovitz and Mackay - FE modelling

A 2-D finite element model using minimisation of elastic energy (and interfacial energy in [51]) has been successful in predicting rafting directions for NASAIR 100 [50,51]. However this Monte-Carlo finite element model was shown to be consistent with Pineau's stability map [51] which suggests it would predict incorrectly for at least one data point and might do the same for a number of others. As in the Socrate and Parks case, the agreement of the 2D model for strongly interacting particles with the 3D model for an isolated inclusion may be largely fortuitous.

Glatzel, Feller-Kniepmeier and Müller - FE modelling

Glatzel and Feller-Kniepmeier [53] also constructed a 2-D plane stress FE model. They calculated stresses in the matrix and precipitates in the absence of an applied stress and in the presence of an applied stress. They claimed agreement with results of Pollock and Argon [47], if one took into account the different misfit and the plane stress assumption as opposed to plane strain assumption reported in [47]. They also claimed that the direction of rafting could be inferred if one assumed growth of the precipitate into areas of least stress.

Later, Muller, Glatzel and Feller-Kniepmeier [54] used FEA to determine internal mismatch stresses for various precipitate morphologies, this time comparing plane strain/plane stress assumptions, anisotropic/isotropic assumptions and 2D/3D assumptions. They found that 2-D isotropic modelling gave qualitatively the same results as the other combinations except when calculating the strain energy for a non-cubic morphology. In this the anisotropic model was required.

Ganghoffer et al - FE modelling

Ganghoffer et al [52] have also set up a 2-D, plane stress, FE model. They calculated internal mismatch stresses, considering (i) high and low temperature stress distributions, (ii) the effect of anisotropy and (iii) the effect of plastic flow.

In (i) they observed that the decrease in magnitude of elastic constants at high temperature was balanced by the increase in the misfit magnitude and they observed, not surprisingly, that the stresses in the matrix changed sign at high temperature as a result of the change in sign of δ . In (ii) they observed that the effect of anisotropy is to increase the stress levels. In (iii) they saw most plastic strain in the middle of the channel and at the corner of the precipitate.

I.4 The Purpose of this Study

It is clear that the reduction of the elastic energy stored in an alloy is an important driving mechanism for rafting. In the presence of an applied stress, what is important, is the reduction of the total energy of the system (alloy plus loading mechanism). In section I.3 it was seen that 3-D models appropriate to low γ' volume fraction alloys have been developed and 2-D models appropriate to high γ' volume fractions have been developed. No 3-D rafting models appropriate to a high γ' volume fractions appear to have been presented.

The aim of this study is to develop a simple, purely elastic, 3-D model appropriate to an anisotropic alloy with a high γ' volume fraction. The model will be used to :

- a. provide information on the problem of rafting in the absence of applied stress in a high γ' volume fraction alloy. As discussed in I.3, this cannot be dealt with in a 2-D model.
- b. investigate the purely elastic contribution to the rafting process in a high γ' volume fraction alloy.
- c. predict the direction of rafting in various Ni-based superalloys.

Rafting will be investigated by doing an elastic stability analysis of the initially observed cuboids. Only small perturbations of shape from cuboidal are thus considered. The 'flattening' of a cuboid into a plate and the 'lengthening' of a cuboid into a rod will be characterised by a single parameter. The change in elastic energy with respect to this parameter will then be determined.

When the shape parameter is zero, i.e for a cuboidal precipitate, the nature of this change in energy will be investigated and any information on the role of elastic energy in rafting will be extracted. The direction of rafting for a particular alloy will be given by the sign of the quantity. The stability analysis will be done, firstly, for the case where no external stress is applied and secondly for the case where an external stress is applied.

Chapter II

A New Model for Rafting

II.1 Outline of the model

In a typical Ni-based superalloy that is fully aged one sees an array of cuboidal γ' precipitates embedded in a γ matrix, shown here in Fig II.1

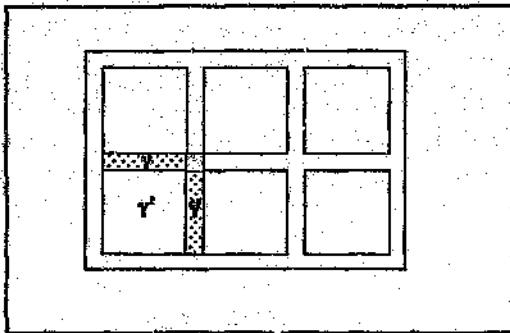


Fig II.1 Schematic diagram of alloy

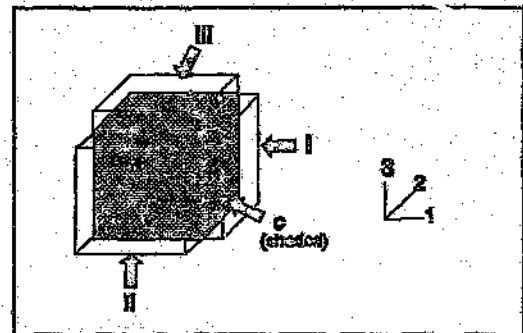


Fig. II.2 The unit volume considered in this model

A modern alloy has a γ' volume fraction in the range 0.6 to 0.7 so that the thickness of the γ channels is in the range of 0.1 to 0.2 times the length of the γ' precipitate. In the model proposed here, the shaded square at the cross over of the γ channels is ignored and only the slabs that are 'stuck' onto the sides of the cube and the cube itself are considered in the elastic energy calculations. This seems an acceptable approximation when one considers that the neglected γ regions make up only about 5% of the total volume and that phase transformations during rafting occur only in other regions.

Fig II.2 gives a 3-D picture of the unit volume considered in this model. Slabs normal to directions 1, 2 and 3 are denoted I, II and III respectively. The cuboidal γ' is labelled c.

The strains in the slabs and the cube that are required for coherency depend on the dimensions of the cube and the slabs, on the difference in the unconstrained lattice parameters of γ and γ' and on the difference in their elastic constants. Four variables have been defined to describe this dependence:

$$T = \frac{t}{w} \quad (1)$$

where t is the thickness of the plate and w is the length of the precipitate (in the unconstrained state);

$$\delta = 2 \frac{(a' - a)}{a' + a} \quad (2)$$

where a and a' are the lattice parameters of γ and γ' respectively;

$$m = \frac{c'_{11}}{c_{11}} - 1 \quad (3)$$

$$n = \frac{c'_{12}}{c_{12}} - 1 \quad (4)$$

where the C_i 's are elastic constants. Note that C_{44} does not occur.

To determine the stresses and strains in the slabs and in the cube one can consider what they look like in the unconstrained state. Fig II.3 illustrates, in 2-D, the case where the γ' is elastically much harder than the γ phase and the unconstrained lattice parameter of the γ' is smaller than that of the γ . Stated in terms of the variables defined above, Fig II.3 illustrates the case of negative δ and large positive m and n . For coherency in this case, the slabs need to be squeezed onto the sides of the cube, the dimensions of the cube changing very little.

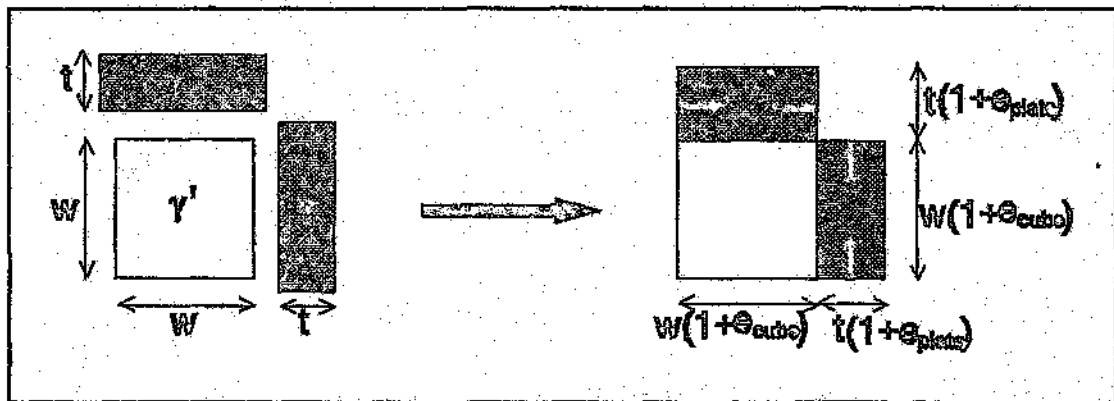


Fig. II.3 The assembly of slabs and cube to form the configuration observed. Uniform strains assumed.

Of course, if the γ' cube were elastically much softer than the γ plates (m and n negative) and δ was still negative then it would be the γ' cube that would stretch to fit the plates. In practice the elastic constants of the γ' and the γ are similar, that is $|m|$ and $|n|$ are about 0.1.

General Procedure for Elastic Energy Calculation

It is assumed that each component of the unit volume shown in Fig. II.2 is uniformly strained. One can then use equilibrium conditions to obtain an approximation to the stresses and strains in the precipitate and the matrix slabs when they are constrained in the alloy. Strains will be accurate up to terms linear in T . (T^2 terms cannot be considered since the γ channel cross overs have been neglected).

Internal strains must contain a factor of δ in all terms while strains resulting from an applied stress, σ , must contain a factor of σ/c_{11} in all terms. These are both small quantities - in the region of, or less than, $\pm 0.1\%$. The internal strains that are calculated can then be accurate up to terms containing the product of δ and one of the small quantities T, m or n . Strains resulting from an applied stress can be accurate up to terms containing the product of σ/c_{11} and one of the small quantities T, m or n .

Elastic energy densities can then be calculated and the energies for each component can be determined. By summing the energies calculated for each component, an approximation to the elastic energy stored in a unit volume of the superalloy can be obtained. It should also be possible to investigate the work done by an externally applied stress. The smaller T, m and n are, the better the energy approximations will be. A small T corresponds to large γ' volume fraction so the model should provide a method for investigating elastic energies in high γ' volume fraction alloys.

II.2 Elastic Stability Analysis in the Absence of Applied Stress

To do an elastic stability analysis for the cube/slab configuration one considers the disassembled state of cube and slabs shown in Fig II.4. The 3-axis lies vertical in the plane of the page. During plate formation a layer of γ' normal to the 3-axis transforms to layer of γ . At the same time layers of γ parallel to the 3 axis transform to γ' . The diagram is shown in 2-D but the plate shown parallel to the 3-axis is, of course, equivalent to the other parallel plate.

The volume of γ' stays roughly constant during rafting. The volume of material transformed on the two parallel faces must therefore be roughly the same as the material transformed on the normal face. Thus, when the cube loses a thickness of $2\epsilon w$ on the normal face it must gain ϵw from each parallel face. The two phases, of course, have different unconstrained lattice parameters and thus unconstrained γ' of width ϵw will have width $\epsilon w a/a'$ after it has transformed to unconstrained γ (a represents the lattice parameter).

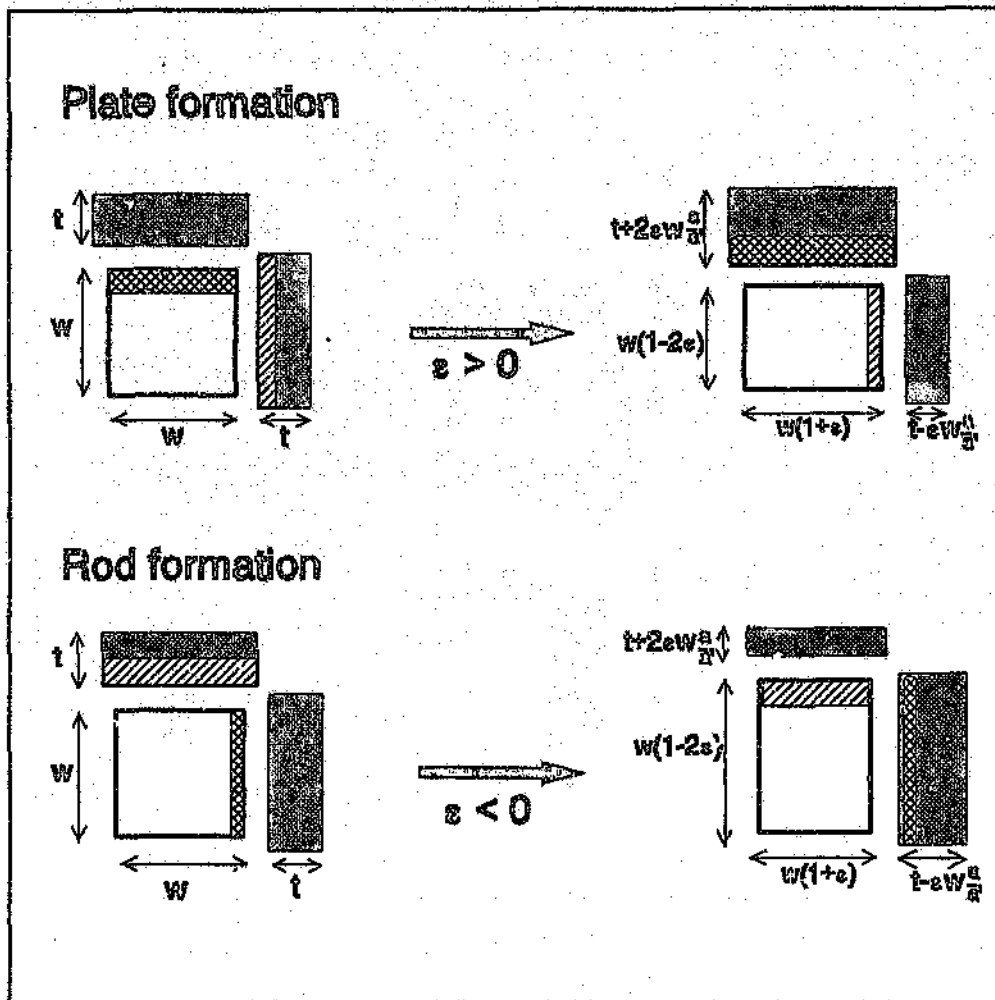


Fig.II.4 Changes in unconstrained slab and cube dimensions when rafting occurs. The 3-axis is vertical in the plane of the page.

In Fig II.4 a useful shape parameter has been defined: when ϵ is positive it describes plate formation; when it is negative it describes rod formation. Fig II.4 also illustrates the consequences of an important assumption made in the model presented here: that the two phases are perfectly coherent before and after rafting.

The reassembled sets of slabs and cubes are shown in Fig.II.5. The uniform strains that are required for coherency are denoted

$$e_p^{qr}$$

where

$p = 1,2,3$ and gives the direction of e , the principal strain

$q = I,II,III,c$ and gives the component in which the strain appears and

$r = i, a$, denoting whether the strain is an internal strain or a strain resulting from an applied stress.

Stresses are labelled in a similar manner.

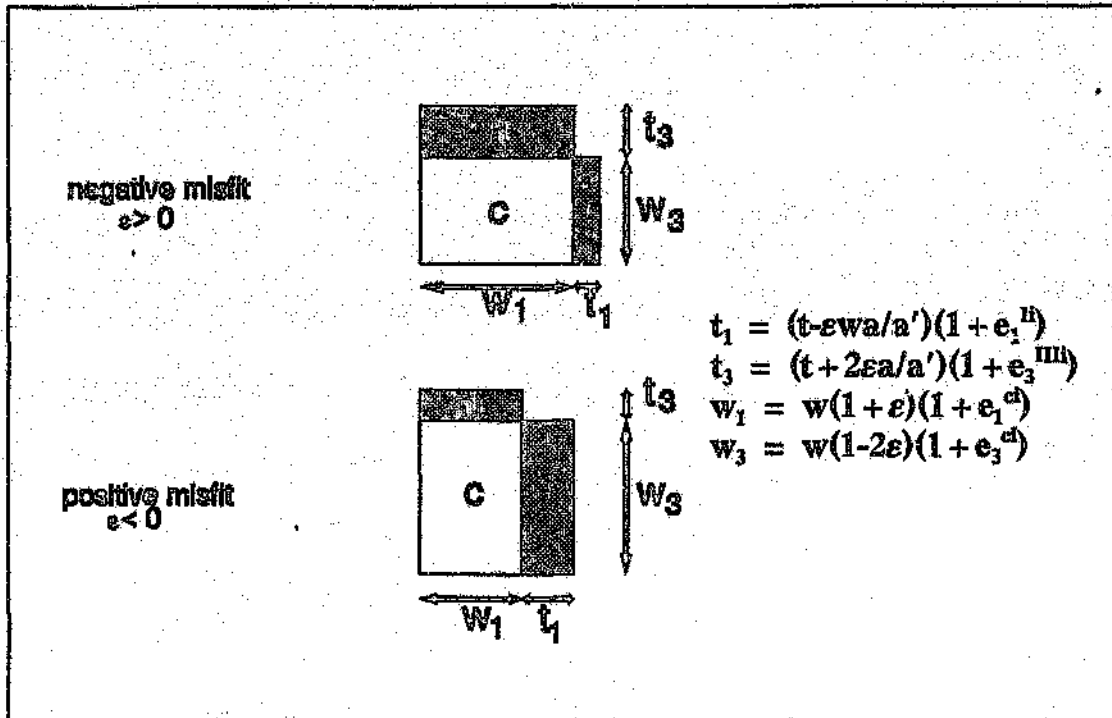


Fig.II.5 Assembled state of slabs and cube.

In each of the three slabs and the cube there are three principal strains to determine - 12 strains in all. There are also 12 principal stresses but these are, of course, related to the strains through the generalised Hooke's law equations. By the symmetry of the problem:

- * the strains in the I slab give those in the II slab (3 conditions);
- * both in the cube and in slab III, the 1 and 2 directions are equivalent (2 conditions);
- * the strain in the 1 direction in the III plate is the same as that in the 1 direction in the II plate (1 condition)

Continuity of normal stresses across the slab I/cube interface gives:

$$P_1^{II} = P_1^{cI} \quad (5)$$

Continuity of normal stresses across the slab III/cube interface gives:

$$P_3^{III I} = P_3^{c I} \quad (6)$$

Cancellation of forces on a plane normal to the 3-axis gives:

$$P_3^{c I} w_1^2 + 2P_3^{I I} w_1 t_1 = 0 \quad (7)$$

Cancellation of forces on a plane parallel to the 3-axis gives:

$$P_2^{I I} w_3 t_1 + P_2^{III I} w_1 t_3 + P_2^{c I} w_1 w_3 = 0 \quad (8)$$

The eleventh and twelfth conditions are given by the misfit relationship between strains in the cube and in the slabs. In the constrained state the cube and slabs must 'fit' in the 1-direction and in the 3-direction, that is, the constrained lattice parameter in the 1-direction in the cube is the same as that in the 1-direction in slab III; and the constrained lattice parameter in the 3-direction in the cube is the same as that in the 3-direction in slab I.

Labelling the new constrained parameter in the 1-direction a_{n1} , one gets

$$e_1^{c I} = \frac{a_{n1}}{a'} - 1 \quad e_1^{I I} = \frac{a_{n1}}{a} - 1$$

and similarly for the 3-direction.

To second order equation (2) gives

$$\frac{a}{a'} = \left(1 - \delta + \frac{\delta^2}{2}\right)$$

This gives the following relations between strains in the cube and strains in the slabs:

$$e_1^{c I} = (1 + e_1^{III I}) \left(1 - \delta + \frac{\delta^2}{2}\right) - 1 \quad (9)$$

$$e_3^{c I} = (1 + e_3^{I I}) \left(1 - \delta + \frac{\delta^2}{2}\right) - 1 \quad (10)$$

Neglecting (strain)² and higher order terms, the equations can then be solved for all stresses and strains. These are expanded binomially. As discussed in II.1, terms containing the product of δ and more than one of T, m or n are neglected.

The elastic energy density in each slab and in the cube can then be determined by

$$u^x = \frac{1}{2} \sum_i p_i^x e_i^x \quad (11)$$

where $i = 1, 2, 3$ and $x = c, I, III$ and the p 's and e 's are principal stresses and strains.

The total elastic energy of the unit volume is then given by

$$E = u^c V^c + u^{III} V^{III} + 2u^{I} V^I \quad (12)$$

where the V 's represent the volumes of the components. In calculating the volumes the (1+strain) factors shown in Fig.5 were not included since these would only contribute

(strain)³ terms to the energy. The smallest terms that are included in the energy are the products of δ^2 and T, m or n - higher order terms are neglected.

The change in energy with respect to shape parameter when the precipitate is cuboidal can then be evaluated by differentiating E with respect to ϵ and then setting ϵ equal to zero. A negative value for this quantity indicates that the energy decreases with *increasing* ϵ and plate formation is favoured. A positive value indicates that energy decreases with *decreasing* ϵ and rod formation is favoured. If the cube represents a stationary point on the E vs. ϵ curve then the quantity will be zero.

II.3 Stability Analysis in the Presence of an Applied Stress

Once again the disassembled set of slabs and cube is considered but this time with a stress applied in the 3-direction. Fig. II.6 shows how the rafting process is modelled for a negative misfit alloy. In the disassembled state a layer of γ' with thickness $2\epsilon w(1 + e_3^{ca})$ normal to the applied stress transforms to γ . Once it has transformed, it strains like the γ and thus has a thickness $2\epsilon w(1 + e_3^{ma})a/a'$. In each of the two vertical slabs parallel to the 3-axis, a layer of γ with thickness $\epsilon w(1 + e_1^{ln})a/a'$ transforms to γ' . In the transformed state the layers have thickness $\epsilon w(1 + e_1^{ca})$.

The strains required to reassemble the system are just the internal strains calculated earlier, resulting in the last configuration shown in Fig. II.6. Once again there are 12 strains to be calculated with 12 relations between stresses and strains given by the generalised Hooke's law.

Symmetry considerations give:

- * strains in the I plate give those in the II plate (3 conditions)
- * 1 and 2 directions are equivalent in the cube and the III plate. (2 conditions)

The I and II slabs are required to 'fit' onto the side of the cube even after an external stress is applied. This gives two more boundary conditions:

$$* \quad e_3^{ln} = e_3^{ca} \quad (13)$$

$$* \quad e_2^{ln} = e_2^{ca} \quad (14)$$

After the external stress is applied Slab III horizontal to the applied stress is required to 'fit' onto the the cube and slabs I and II. This implies:

$$* \quad e_1^{mha} = (e_1^{ln}t_1 + e_1^{ca}w_1)/(w_1 + t_1) \quad (15)$$

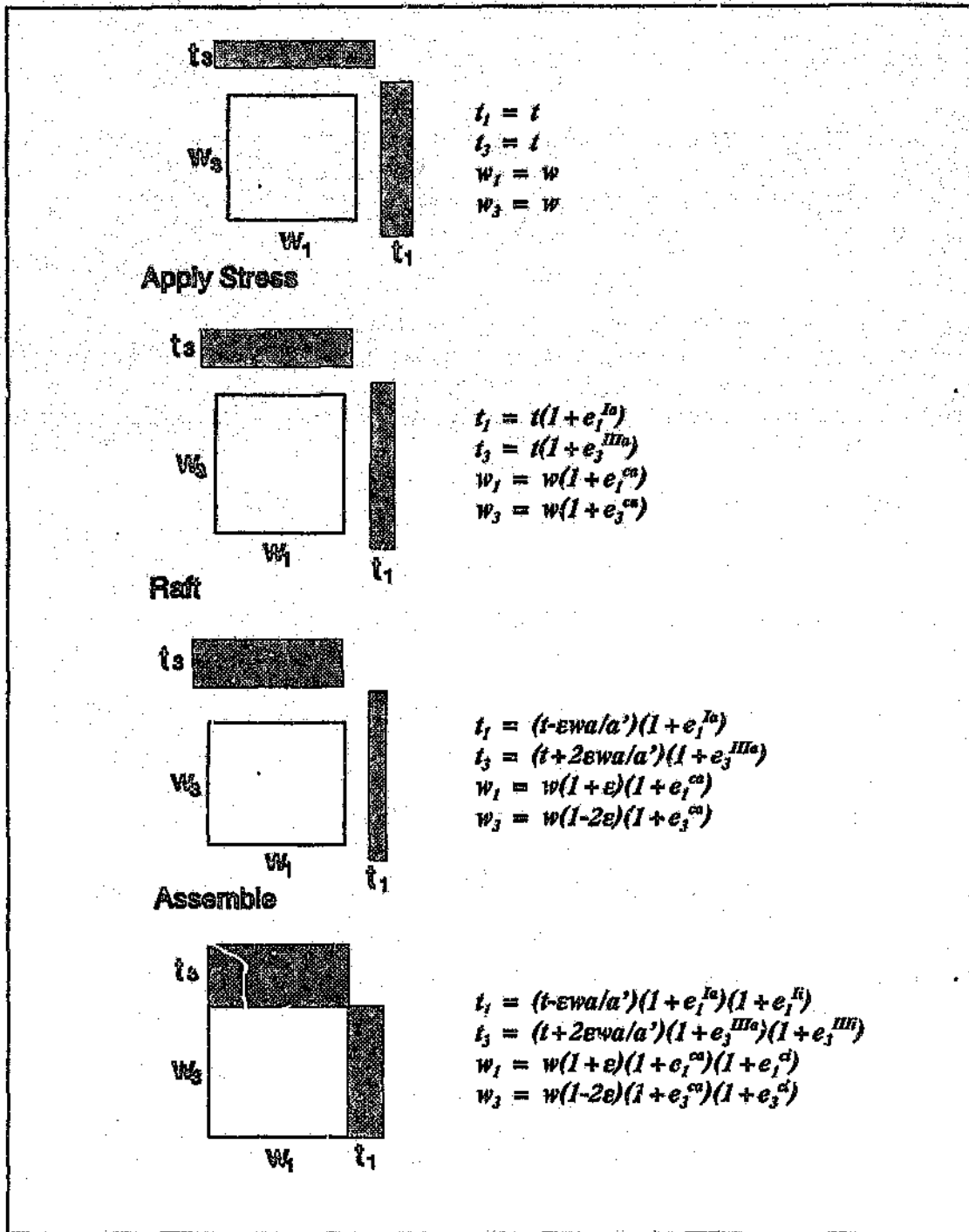


Fig.II.6 Rafting under applied stress - disassembled and assembled configurations

Equilibrium constraints give

$$* \quad p_1^{Ia} = p_1^{cI} \quad (16)$$

$$* \quad p_3^{IIIa} = p_3^{ca} \quad (17)$$

$$* \quad \sigma(w_1+t_1)^2 = p_3^{ca}w_1^2 + 2p_3^{In}w_1t_1 \quad (18)$$

$$* \quad p_1^{ca}w_1w_1 + p_2^{In}w_3t_1 + p_1^{IIIa}w_1t_3 = 0 \quad (19)$$

Equation (16) and (17) are obtained from the requirement that normal stresses be continuous across cube/slab interfaces. Equation (18) is obtained from the requirement that the average force on the plane normal to the 3-axis be the applied stress multiplied by the area over which it acts. Equation (19) results from the requirement that the average force on the plane parallel to the 3-axis be zero.

Once again all (strain)² and higher order contributions are neglected and one can solve for strains and stresses resulting from an applied stress. As discussed in II.1, all terms containing the product of σ/c_{11} and more than one of T,m or n are also neglected. The elastic energy density can be calculated using the total (denoted by a (T) superscript) stresses and strains in the following way:

$$u^x = \frac{1}{2} \sum_j p_j^{(T)x} e_j^{(T)x} \quad (\text{where } x=I, III, c)$$

where

$$p_j^{(T)x} = p_j^{(a)x} + p_j^{(i)x} = (\text{applied stress})_j^x + (\text{internal stress})_j^x$$

and

$$e_j^{(T)x} = e_j^{(a)x} + e_j^{(i)x} = (\text{applied strain})_j^x + (\text{internal strain})_j^x$$

Thus the total elastic energy density in each component of the system is given by

$$u^x = \frac{1}{2} \sum_j (p_j^{(a)x} e_j^{(a)x} + p_j^{(a)x} e_j^{(i)x} + p_j^{(i)x} e_j^{(a)x} + p_j^{(i)x} e_j^{(i)x}) \quad (20)$$

The total elastic energy for the system can again be calculated using (12):

$$E^T = u^c V^c + u^{III} V^{III} + 2u^I V^I$$

As for the case of no applied stress, the (1+strain) factor appearing in the widths and thicknesses are ignored for volume calculations as they contribute only (strain)³ terms to the energy.

When determining the energy for this system, one must consider the potential energy of the external loading mechanism. Thus it is the change in the enthalpy with respect to ϵ that is of interest. The enthalpy is given by elastic energy minus the work done. The work done is calculated in the following way:

$$W = F \cdot d = \sigma \cdot A \cdot d \quad (21)$$

where

$$A = (w_1 + t_1)^2 \quad (22)$$

and

$$d = e_3^{ca} w + e_3^{IIIa} t \quad (23)$$

Again (strain)³ and higher order terms are ignored. The smallest terms that are included in the enthalpy are terms containing the products of (σ/c_{11}) and T, m or n and products of δ and T, m or n.

If

$$\left. \frac{\partial (E-W)}{\partial \varepsilon} \right|_{\varepsilon=0}$$

is negative then N-type behaviour is predicted; if it is positive then P-type behaviour is predicted and if it is zero then the cube represents a stationary point.

Chapter III

Results

III.1 Internal Stresses Calculation

The calculations outlined in Chapter 2 involved large equations that were manipulated using the symbolic maths package, Maple.

The internal stresses were calculated for the configuration shown in Fig.II.5. When $\epsilon=0$ the stresses calculated are just those of the cube configuration and can be checked against finite element calculations [52,54,48] of internal stresses in various superalloys. This is shown in Table III.1. Since strains are not uniform in the FE calculations, the values given halfway between the midpoint of the slabs and the corner are used. The subscript 'vm' indicates a von Mises equivalent stress.

It is important to note that values obtained for SRR 99 and for CMSX-2 using the finite element method were done under plane stress assumptions. Plane strain assumptions give a better approximation to the real values [48,54] and lead to stresses that are about 1/2 more than those obtained under plane stress assumptions [53,59]. Values for what one might thus obtain under plane strain assumptions are shown in brackets in the table

Table III.1 Calculated values of internal stresses compared with those obtained in FE analyses

Alloy	Source	p_2^H (MPa)	p_1^H (MPa)	p_{vm} in γ (MPa)
CMSX-3	Model	-430	130	560
	[48]	-460	40	465
SRR 99	Model	-210	80	290
	[54]	-	-	~ 180 (270)
CMSX-2	Model	-247	102	349
	[52]	-	-	~ 190 (285)

In the model developed in this dissertation the von Mises stresses are zero in the γ' cube. Non-zero values arise in the models listed above as they are not confined to a uniform strain approximation.

The results do not show excellent agreement but they are still encouraging.

III.2 Internal Energy Calculations

It was found that the cube-shaped precipitate represents a stationary point on the elastic energy vs ϵ curve, that is:

$$\left. \frac{\partial E}{\partial \epsilon} \right|_{\epsilon=0} = 0$$

to the order used in this model. This is in agreement with the results for isolated ellipsoidal particles studied by Miyazaki et al [20] and Johnson et al [55]. Unfortunately the approach used in this study does not yield the nature of the stationary point but much insight can be gained from the two studies mentioned above. This will be discussed in the next chapter.

III.3 Calculation of Elastic Energy Changes in the Presence of Applied Stress

The applied strains in the slabs and cube shown in the final configuration of Fig II.6 were determined. As is expected, the applied strains in slab III (the horizontal slab) differed from the those in the vertical slabs and in the cube by an amount proportional to m and n.

The change in elastic energy with respect to the shape parameter ϵ is given below in eq.III.1

$$\left. \frac{\partial (E-W)}{\partial \epsilon} \right|_{\epsilon=0} = \frac{[2(c_{11}^2 + c_{11}c_{12})m - 4c_{12}^2n] \sigma^2 K + [2c_{11}c_{12}(c_{11} - 4c_{12})n + 2c_{11}^2(c_{12} + 2c_{11})m + 2(c_{12}c_{11}^2 + 4c_{12}^3 + 3c_{11}^3 - 8c_{11}c_{12}^2)T] \sigma \delta K}{1} \quad (1)$$

$$\text{where } K = \frac{w^3}{c_{11}(c_{11}^2 + c_{11}c_{12} - 2c_{12}^2)}$$

It should be noted that although the T appearing here is strictly the the ratio of the channel thickness to cube length in the *unconstrained* state, the internal strains are small are enough for t/w in the constrained state to be considered equal to T.

Data in Table 1 indicate that the differences between m and n are certainly not larger than 30%. Taking $n=m$ in the above equation III.2 simplifies the expression greatly. One obtains:

$$\left. \frac{\partial (\epsilon - WK)}{\partial \epsilon} \right|_{\epsilon=0} = \left(2m \frac{\sigma^2}{c_{11}} + 2\delta \sigma \left[2m + T \left(3 - 2 \frac{c_{12}}{c_{11}} \right) \right] \right) w^3 \quad (2)$$

Table I.1 contains complete sets of data for four alloys and almost complete sets for two others. For the two almost complete sets c_{11} is set equal to 100 GPa and c_{12} is set to 0.64 of c_{11} . The data is then substituted into equations 1 and 2 to obtain predictions of rafting direction for the six alloys. The data used is shown in Table III.2 and the results are shown in Table III.3. When substituting into equation 2 an average of the m and n values given in Table III.2 is used in place of m . It should be noted that the volume fractions of Udimet 700 and for Ni-15Al are probably too small to obtain accurate results but the predictions are still of interest.

Table III.2 Data used to obtain results in Table III.3

Alloy	m	n	t/w	$\delta(\%)$	σ (MPa)	c_{11} (GPa)	c_{12} (GPa)
CMSX-3	-.11	-.14	.13	-.38	150	202	139
CMSX-2	.15	.14	.13	-.33	120	109	59
SRR 99	.10	.03	.13	-.21	170	187	129
Ni-15Al	.49	.68	.5	+.56	147	112	63
Udimet	~-.1	~-.1	.4	-.3	147	~100	~.64 c_{11}
NASAIR	~.12	~.12	.19	-.45	148	~100	~.64 c_{11}

Table III.3 Results of substitution into equations 1 and 2

Alloy (tens/comp)	$\frac{\partial(E-WK)}{\partial e} \Big _{z=0}$ per (unit vol*10 ⁶) [eq1]	$\frac{\partial(E-WK)}{\partial e} \Big _{z=0} \quad (n=m)$ per (unit vol*10 ⁶) [eq2]	Rafting Observed
CMSX-3 (T)	-0.05	+0.01	N
CMSX-2 (T)	-0.4	-0.4	N
SRR 99 (T)	-0.3	-0.2	N
Ni-15Al (T)	+3	+3	P
Ni-15Al (C)	-3	-3	N
Udimet (T)	-0.5	-0.5	N
Udimet (C)	+0.4	+0.4	P
NASAIR (T)	-0.7	-0.7	N
NASAIR (C)	+0.8	+0.8	P

Chapter IV

Discussion

IV.1 The Internal Energy Result.

The effect of interfacial energy has not been considered. Marsh and Chen [83] have collected many values for the interfacial energies given in the literature. The values vary with temperature and composition but their survey indicates that $0.01\text{J}\cdot\text{m}^{-2}$ is an acceptable estimate at 800°C . Thus, using a precipitate size of $0.3\mu\text{m}$:

$$E_{if} = \gamma \cdot A \approx 0.01\text{J}\cdot\text{m}^{-2} \cdot 6 \cdot (0.3 \cdot 10^{-6}\text{m})^2$$

This gives a value for the interfacial energy of about $0.54 \times 10^{-14}\text{J}$. Calculations of the internal elastic energy using the model here give values of about $4.6 \times 10^{-14}\text{J}$. Thus for precipitates of this size the internal elastic energy is about an order of magnitude larger than the interfacial energy and the effects of interfacial energy should, therefore, be small. This is supported by results discussed in II.3 [20,55,78].

In section III.2 it was reported that the model proposed in this dissertation leads to the conclusion that the cube is a stationary point on the elastic energy vs. shape parameter curve. The stationary point represented by the cube could be a minimum. Studies of isolated inclusions by Miyazaki et al [20] and Johnson et al [55] suggest something different. They consider interfacial energy in their studies. For small precipitates, the sphere represents a minimum on their energy vs. shape curves since interfacial energy effects will dominate over elastic energy effects then. At larger sizes the elastic energy dominates and plate shaped particles represent a global minimum on their curves. They also find, though, that the sphere represents a stationary point on the energy vs. shape curve, *even when elastic energy dominates over interfacial energy*; in this case, however, the sphere represents a local maximum.

In high γ' volume fraction alloys, it is generally observed that precipitates evolve towards a cuboidal shape during ageing, even when the size of the precipitates is not changing. This suggests that the stationary point represented by the cube is in fact a minimum on the elastic energy vs. shape parameter curve in high γ' volume fraction alloys. It seems likely that the plate morphology will also represent a minimum on the curve as was found for isolated inclusions. Nabarro has suggested that for a high ratio of surface to elastic energy the cube will represent a deeper minimum than the plate; when surface energy is less important, the plate minimum will be deeper.

It makes sense, then, that during ageing of an alloy, spherical precipitates will coarsen until the effects of elastic energy start becoming large. Generally, cuboids will be favoured elastically. If the plate morphology represents a deeper minimum than the cube morphology, imperfections in the microstructure will permit the precipitates to evolve towards the lower energy plate morphology.

IV.2 Interpretation of the Full Applied Stress Result.

The results given in the last chapter can be interpreted in the following way:

The σ^2 term:

A σ^2 term appears in the expression for the enthalpy of the final configuration shown in Fig.II.6. The term represents the enthalpy that results only from the applied stress and not from any interaction between internal and external stresses. Thus, in eq.III.1, the σ^2 term represents the change in this enthalpy when rafting starts.

It was pointed out in III.3 that if the alloy were homogenous ($m=n=0$) then the material would strain uniformly under an applied stress. That is, in Fig.IV.1 layer A strains by the same amount as layer B. This is not so in the inhomogeneous case: the strains in layer A will differ from those in layer B by an amount that depends on the difference in the elastic constants between the two phases.

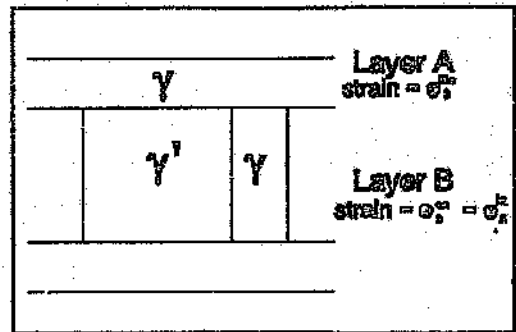


Fig.IV.1 Strains resulting from applied stress

The strain energy density resulting only from the applied stress will thus be the same in both layers for the homogenous case but not for the inhomogeneous case. Thus, the corresponding energy will not change on rafting for the homogenous case but will for the inhomogeneous case.

When m and n are not zero, the coefficient of σ^2 is

$$K[2(c_{11}^2 + c_{11}c_{12})m - 4c_{12}^2n]$$

where K is given in eq.III.3. One sees that K is always positive since c_{11} is positive and always greater than c_{12} . The sign of the σ^2 term is thus given by the sign of m unless

$$n > \frac{1}{2} \left(\frac{c_{11}^2}{c_{12}^2} + \frac{c_{11}}{c_{12}} \right) m$$

and n is the same sign as m .

Taking $c_{12}/c_{11} \approx 0.64$ (an average of values given in Table 1) $|n|$ must be greater than about $2|m|$ and the same sign as m before the sign of the σ^2 term is given by minus the sign of m . Physically this corresponds to the situation where strains resulting from Poisson effects start influencing the energy change during rafting more than the strains in the direction of the applied stress.

The $\sigma\delta$ term

A $\sigma\delta$ term appears in the expression for the enthalpy of the last configuration shown in Fig. II.6. This term presumably results from the interaction energy between internal and external stresses. The $\sigma\delta$ term appearing in eq. III.1 is thus the change in this interaction energy that occurs during rafting.

Taking $m=n=0$, one obtains the extreme case of a homogenous, misfitting precipitate with a dilatational strain. Nabarro considered a 2-D model of homogenous slabs and cubes. With Poisson effects neglected (implies $c_{12}=0$), it was shown that the shape of the precipitate-slab combination did not change during rafting. This implies that an applied stress does no work during the rafting process for this 2-D model. If this were shown to be true for the 3-D model proposed in this dissertation, one would expect the change in energy on rafting in the homogenous case to be zero. A term in $T\sigma\delta$ would then surely indicate an error in the calculations. This is discussed further in IV.5.

It should be noted that experimental results suggest the presence of a term that does not contain m or n . Table I.1 shows that negative misfit alloys display the same rafting behaviour even when soft precipitates (CMSX-3 and Udimet 700) and hard precipitates (NASAIR 100, SRR 99, CMSX-2) are considered. This would not be predicted if the $T\sigma\delta$ term were absent. However, elastic constant data are definitely unreliable - as will be discussed below - and one is not guaranteed that precipitates are, in fact, hard or soft. It is also possible that inelastic effects might be enough to reverse the effects of the elastic driving force.

It was pointed out in II.2 that the model is not valid for the case of $T=0$. However, it is not difficult to understand the physical significance of terms in $\sigma\delta m$ and $\sigma\delta n$. As in the discussion of the σ^2 term, the differences in elastic constants result in different applied strains in layer A and layer B shown in Fig. IV.1. On rafting, these result in differences in $\sigma\delta$ terms in the enthalpy.

More insight can be gained into the physical conditions which result in a negative or positive contribution from the $\sigma\delta$ term by considering the approximate form for eq. III.1. Some observations can be made here, though: the coefficient of $T\sigma\delta$ is always positive, as is T . The coefficient of m is also always positive and always larger than the coefficient of n . The coefficient of n will be negative unless $c_{12}/c_{11} < 1/4$.

IV.3 The Approximation $m=n$

The most obvious feature of the predictions made using the approximate form of eq. III.1 is that it does not predict correctly for CMSX-3. It should be noted that the prediction for CMSX-3 made using the full equation is an order of magnitude smaller than the other predictions. This agrees well with the unusually slow rafting rate in CMSX-3 that was discussed in II.3. The small value predicted is a result of the $\sigma\delta$ terms nearly cancelling. In the approximate form, it appears that when these terms are so close to cancelling, the differences in n and m are significant.

The σ^2 term:

The approximate form for eq.III.1, given in eq.III.2 is easier to understand physically.

The sign of the σ^2 term is always given by the sign of m . Thus, a soft precipitate will always generate a term promoting N-type rafting and a hard precipitate will always generate a term promoting P-type rafting.

Eq.III.2 gives the critical stress at which the σ^2 term becomes dominant as

$$\sigma = \pm \delta \left(2m + T \left(3 - 2 \frac{c_{12}}{c_{11}} \right) \right) \frac{c_{11}}{m}$$

It should be noted that in the alloys shown in Table III.2 (apart from CMSX-3) this term would only begin to dominate when σ was of the order of 1 GPa. In CMSX-3 the critical stress is an order of magnitude smaller and thus it would appear that the σ^2 term could play a more important role for this alloy. In general, however, the effects of the $\sigma\delta$ term are of more interest.

The $\sigma\delta$ term:

The $\sigma\delta m$ term has a factor of 2δ where the σ^2 term has a factor of σ/c_{11} . Using Table III.2, the $\sigma\delta m$ term is 4 to 10 times the size of the σ^2 term. The magnitude of $T\sigma\delta$, meanwhile, is about 1 to 2 times that of the $\sigma\delta m$ term.

For $m > -T(3/2 - c_{12}/c_{11})$ (The Common Region):

In this case the coefficient of $\sigma\delta$ is always positive and, as long as it is larger than the σ^2 term, one will observe the usual rafting phenomenon: in a negative misfit alloy, P-type under compression and N-type under tension; in a positive misfit alloy, P-type under tension and N-type under compression.

The σ^2 term contribution is to increase the tendency toward P-type rafting when m is positive and increase the tendency toward N-type rafting when m is negative. As pointed out above this should not be a large contribution for alloys in Table III.3 (except CMSX-3);

For $m < -T(3/2 - c_{12}/c_{11})$ (The Sign Reversal Region)

In this case the sign of the $\sigma\delta$ term is reversed. For cases where P-type rafting was predicted above, N-type rafting is predicted and vice versa. The critical value of m when the coefficient of $\sigma\delta$ begins to introduce a minus sign is around -0.15 (using an average of data given in Table III.2).

IV.4 Unreliable Elastic Constants

The composition of three of the four alloys with full sets of data available are shown in Table IV.1. MAR-M200 is also shown as elastic constants for SRR 99 are based on MAR-M200

Table IV.1 Composition of alloys

Alloy	Ni	Ti	Ta	Al	Cr	W	Co	Mo	Hf
CMSX-3	67.9	1.1	1.9	12.4	9.1	2.6	4.7	0.3	.03
CMSX-2	67.3	1.25	2.0	12.2	9.2	2.6	5.1	0.31	-
NASAIR	69.6	1.5	2.8	5.7	9.2	10.2	-	1.0	
SRR 99	66.5	2.2	2.8	5.5	8.5	9.5	5.0	trace C	
MARM200	60.3	2.0	-	5.0	9.0	12.5	10	Nb 1.0 trace B,C	

One sees an overwhelming similarity between CMSX-3 and CMSX-2. Yet Pollock and Argon claim that CMSX-3 [48] has elastically soft precipitates while Ganghoffer et al claim that CMSX-2 has elastically hard precipitates [52].

The matrix constants for CMSX-3 were taken to be the constants of the bulk material; constants of the γ' were obtained by extrapolating Curwick's data [84] for $\text{Ni}_3\text{Al} + \text{Ta}$, assuming a temperature dependence similar to that of the matrix. Ganghoffer et al collected data for Young's modulus in the $\langle 001 \rangle$ directions which were measured at different temperatures up to 1100°C . Poisson's ratio was taken to be independent of temperature and equal to 0.35 in both phases.

Gayda and MacKay measured Young's modulus along $\langle 001 \rangle$ directions in NASAIR 100 at 25°C , 500°C and at 1000°C . They found that at low temperatures the γ was harder than the γ' but that at higher temperatures the γ' became harder. Müller et al [54] reported similar behaviour using elastic constants that had been determined for MAR-M200 using the Förster resonance method.

Ganghoffer's results also showed the same change in relative stiffness of the two phases at high temperature. Admittedly, their results depended fairly heavily on Gayda and MacKay's data. MAR-M200 has a some Co substituted for Ni but generally the last three alloys shown in the table are similar and one might expect similar elastic constants for them. However, one would not necessarily expect CMSX-2 to show the same trends.

The only thing that is really clear is that the CMSX-2 and CMSX-3 elastic constants given in the literature are very surprising. The CMSX-3 investigators assumed the same temperature dependence for γ' constants as for γ constants which, it appears, would not be correct for an alloy such as NASAIR 100 or MAR-M200. Whether they have missed a trend present in all alloys or the CMSX-2 investigators have relied too heavily on high W content alloys is not clear.

One could argue that the two alloys also show surprisingly different rafting behaviours for materials that are compositionally so similar. Nevertheless, more investigation seems required and one can only really conclude that elastic constant data are probably unreliable.

IV.5 Reconsidering the Problem

The presence of the suspicious $T\sigma\delta$ term, mentioned above, has led to a closer look at the studies of isolated inclusions that have been done using Eshelby's method [20,21,24]. It appears that in these studies the $\sigma\delta$ term arises in the work calculation and not in the stored energy calculation. This is not the case in the study presented here. While this, in itself, is a major cause for concern, it has also highlighted an omission in the work calculation presented here: in Fig.II.6, it seems that the work done by the external stress during the rafting phase and the assembly phase cannot have been included correctly since the resulting expression is a function of σ^2 .

Unfortunately, it appears that the correct predictions shown in Table III.2 could be largely fortuitous. All the same, a useful first attempt at using this model has been made and much insight has been gained into the problem. Future work will probably include a re-working of the calculations, possibly using the following method given by Nabarro:

	Process 1	Process 2
1.	Take components that will assemble at $\varepsilon=0$	
2.	Keep them	Trim to assemble at $\varepsilon=\varepsilon$
3.	Assemble at $\varepsilon=0, \sigma=0$ Calc. work	Assemble at $\varepsilon=\varepsilon, \sigma=0$ Calc. work
4.	Apply σ , Calc. work	Apply σ , Calc work
5.	Add works	Add works
6.	Difference between 1 & 2 gives driving force	

It has also been suggested that a closer approximation to the observed morphology could be obtained if overlapping slabs were considered. That is, strain energies should be considered for slabs that are longer than the precipitate by half the width of a γ channel (in the unconstrained state).

IV.6 Comparing the Model with Applied Stress Observations

As it stands, the model successfully accounts for the dependence of rafting on the signs and magnitudes of δ and σ , since under conditions normally encountered, the σ^2 terms are small in comparison with the $\sigma\delta$ terms which show the correct sign dependence. The model is consistent with the observation of rafts being about the same thickness as cubes. It also

predicts the difference in stresses between horizontal and vertical channels.

It cannot make predictions about inelastic effects nor about kinetics-linked observations e.g. temperature dependence and rafting rates. (Although the strength of the tendency to raft under elastic stresses when compared with other alloys can be predicted). The model is not instructive for alloys that do not have cuboidal precipitates but it is possible that other slab/precipitate configurations could be considered.

References

1. The Superalloys, eds C.T.Sims & W.C.Hagel, Wiley, New York (1972)
2. Superalloys II, eds C.T.Sims, N.S.Stoloff, W.C.Hagel, Wiley, New York (1986)
3. Ascent to Civilisation, John Gowlett, Knopf Inc., New York, (1984)
4. G.A.Webster & B.J.Pearcey *Met.Sci.J* 1 p97 (1967)
5. C.P.Sullivan, G.A.Webster & B.J.Pearcey *J.Inst.Metals* 96 p274 (1968)
6. W.Danesi & M.Donachie *J.Inst.Metals* 97 p107 (1969)
7. G.A.Webster & C.P.Sullivan *J.Inst.Metals* 95 p138 (1967)
8. G.A.Webster & B.J.Pearcey *Trans. ASM* 59 p847 (1966)
9. A.J.Ardell & R.B.Nicholson *Acta Met.* 14 p1295 (1966)
10. J.M.Oblak, D.F.Paulonis & D.S.Duvall *Metall.Trans.* 5 p143 (1974)
11. D.F.Paulonis, J.M.Oblak & D.S.Duvall *Trans. ASM* 62 p611 (1969)
12. J.K.Tien & S.M.Copley *Metall.Trans.* 2 p215 (1971)
13. J.K.Tien & S.M.Copley *Metall.Trans.* 2 p543 (1971)
14. J.K.Tien & R.P.Gamble *Metall.Trans.* 3 p2157 (1972)
15. C.Carry & J.L.Strudel *Acta Met.* 25 p767 (1977)
16. C.Carry & J.L.Strudel *Acta Met.* 26 p859 (1978)
17. A.Fredholm & J.L.Strudel *Superalloys 1984* AIME p211
18. A.Fredholm & J-L Strudel *Intl.Conf.on High Temperature Alloys: Their exploitable potential*. Preprints, Petten, Netherlands (1985)
19. A.Lasalmonie & J.L.Strudel *Phil.Mag.* 32 (1976)
20. T.Miyazaki, K.Nakamura & H.Mori *J.Mater.Sci* 14 p1827 (1979)
21. A.Pineau *Acta Met.* 24 (1976)
22. J.D.Eshelby *Proc.R.Soc(A)* 241 p376 (1975)
23. J.D.Eshelby *Prog.Solid Mech.* 2 p87 (1961) (Eds I.N.Sneddon & R.Hill)
24. J.C.Chang & S.M.Allen *J.Mater.Res* 6 p1843 (1991)
25. S.Draper, D.Hull & R.Dreshfield *Metall.Trans.* 20A p683 (1989)
26. M.Feller-Kniepmeier & T.Link *Metall.Trans.* 20A p1233 (1989)
27. J.G.Conley, M.E.Fine & J.R.Weertman *Acta Metall.* 37 p1251 (1989)
28. I.L.Svetlov, B.A.Golovko, A.I.Epishin, N.P.Abalakin *Scripta Metall.* 26 p1353 (1992)
29. R.A.Stevens & P.E.J.Flewitt *Mat.Sci.Eng* 37 p237 (1979)
30. D.D.Pearson, F.D.Lemkey & B.H.Kear *Proc. 4th Int. Symp on Superalloys* ASM (Eds J.K.Tien et al) p513 (1980)
31. D.D.Pearson, B.H.Kear & F.D.Lemkey *Creep and Fracture of Engineering Materials and Structure* (Eds B.Wilshire & D.R.Owen), Pineridge Press Ltd, Swansea, UK, p213 (1983)
32. P.Caron & T.Kahn *Mat.Sci.Eng.* 61 p173 (1983)
33. M.Ignat, J.Y.Buffiere & J.M.Chaix *Acta metall.mater* 41 p855 (1993)
34. R.A.MacKay & L.J.Ebert *Scripta Metall.* 17 p1217 (1983)
35. R.A.MacKay & L.J.Ebert *Superalloys 1984* (Eds M.Gell et al) p135 (1984)
36. R.A.MacKay & L.J.Ebert *Metall.Trans.* 16A p1969 (1985)
37. M.V.Nathal & L.J.Ebert *Scripta Metall.* 17 p1151 (1983)
38. M.V.Nathal & L.J.Ebert *Metall.Trans.* 16A p427 (1985)
39. M.V.Nathal & L.J.Ebert *Superalloys 1984* (Eds M.Gell et al) p125
40. M.V.Nathal & L.J.Ebert *Metall.Trans.* 16A p1849 (1985)
41. M.V.Nathal & L.J.Ebert *Metall.Trans.* 16A p1863 (1985)

42. M.V.Nathal *Metall. Trans.* 18A p1961 (1987)
43. M.V.Nathal & R.A.MacKay *Mat.Sci.Eng.* 85 p127 (1987)
44. M.V.Nathal, R.A.MacKay & R.G.Garlick *Mat.Sci.Eng* 75 p195 (1985)
45. M.V.Nathal, R.A.MacKay & R.V.Miner *Metall. Trans.* 20A p133 (1989)
46. T.P.Gabb, S.L.Draper, D.R.Hull, R.A.MacKay & M.V.Nathal *Mat.Sci.Eng.* A118 p59 (1989)
47. T.M.Pollock & A.S.Argon *Acta metall.mater.* 40 p1 (1992)
48. T.M.Pollock & A.S.Argon *Submitted to Acta metall.mater.*
49. S.Socrate & D.M.Parks *Acta metall.mater.* 41 p2185 (1993)
50. J.Gayda & R.A.MacKay *Scripta Metall.* 23 p1835 (1983)
51. J.Gayda & D.J.Srolovitz *Acta metall* 37 p641 (1989)
52. J.F.Ganghoffer, A Hazotte, S.Denis, A.Simon *Scripta Metall.* 25 p2491 (1991)
53. U.Glatzel & M.Feller-Kniepmeier *Scripta Metall.* 23 p1839 (1989)
54. L.Müller, U.Glatzel & M.Feller-Kniepmeier *Acta metall.mater* 40 p1321 (1992)
55. W.C.Johnson, M.B.Berkenpas & D.E.Laughlin *Acta metall.* 36 p3149 (1988)
56. W.C.Johnson, T.A.Abinandanan & P.W.Voorhees *Acta metall.mater.* 38 p1349 (1990)
58. J.C.Chang, Ph.D Thesis, Dept of Materials Science and Engineering, MIT, 1989
59. Y.Nakada, W.C.Leslie & T.P.Churay *Trans.ASM* 60 p223 (1967)
60. J.Petermann *Z.Metallkde.* 62 p324 (1971)
61. G.Sauthoff *Z.Metallkde.* 66 p106 (1976)
62. W.F.Hosford & S.P.Agrawal *Metall. Trans.* 6A p487 (1975)
63. T.Eto, A.Sato & T.Mori *Acta Met.* 26 p499 (1978)
64. J.H.Westbrook *Z.Kristallog.* 110 p21 (1958)
65. T.Miyazaki, H.Imamura, H.Mori, T.Kozakai *J.Mater.Sci* 16 p1197 (1981)
66. M.Doï & T Miyazaki *Superalloys 1984* (Eds M.Gell et al) p543
67. M.Doï, T.Miyazaki & T.Wakatsuki *Mat.Sci.Eng.* 67 p247 (1984)
68. M.J.Kaufman, P.W.Voorhees, W.C.Johnson & F.S.Biancaniello *Metall. Trans.* 20A p2171 (1989)
69. T.Miyazaki, K.Seki, M.Doï, T.Kozakai *Mat.Sci.Eng.* 77 p125 (1986)
70. A.G.Khachaturyan, S.V.Semenovskaya & J.W.Morris Jr *Acta. Met* 36 p1563 (1988)
71. T.Miyazaki & M.Doï *Mat.Sci.Eng.* A110 p175 (1989)
72. M.Doï *Mat. Trans. JIM* 33 p637 (1992)
73. M.Doï & T.Miyazaki *Superalloys 1992* (Eds S.D.Antolovich et al) p537
74. Y.Wang, L-Q.Chen & A.G.Khachaturyan *Scripta Metall.* 25 p1387 (1991)
75. M.McCormack, A.G. Khachaturyan & J.W.Morris Jr *Acta Metall.Mater.* 40 p325 (1992)
76. R.J.Asaro & D.M.Barnett *J.Mech.Phys.Sol.* 23 p77 (1975)
77. S.C.Lin & T.Mura *Phys.Status Solidi (a)* 15 p281 (1973)
78. A.G.Khachaturyan *Theory of Structural Transformations in Solids*, Wiley, Berlin (1983)
79. S.Sadiq & D.R.F.West *Scripta Metall.* 19 p833 (1985)
80. R.Schmidt & M.Feller-Kniepmeier *Metall. Trans.* 23A p745 (1992)
81. K.Robinson *J.Appl.Phys.* 22 p1045 (1951)
82. T.Mura *Micromechanics of Defects in Solids* (Martinus Nijhoff Publishers, The Hague, (1982)
83. C.N.arsh & H.Chen *Acta metall.mater* 38 p2287 (1990)
84. L.R.Curwick, PhD Thesis, Univ of Minnesota, (1972)
85. P.Caron, P.J.Henderson, T.Kahn & M.McLean *Scripta Metall.* 20 p875 (1986)
86. W.Schneider & H.Mughrabi Proc.of 5th Intl.Conf.on *Creep and Fracture of Engineering Materials and Structures*, The Institute of Metals, London, p209 (1993)

87. T.M.Pollock & A.S.Argon in Proc.of 4th Intl.Conf on *Creep and Fracture of Engineering Materials and Structures*, The Institute of Metals, London, p287,(1990)
88. T.M.Pollock & A.S.Argon *Superalloys 1988* (Eds. S.Reichman et al) p285

Author: Cress Catherine Marion.

Name of thesis: Using elastic energy considerations to explain rafting in Ni-based superalloys with a high gamma volume fraction.

PUBLISHER:

University of the Witwatersrand, Johannesburg

©2015

LEGALNOTICES:

Copyright Notice: All materials on the University of the Witwatersrand, Johannesburg Library website are protected by South African copyright law and may not be distributed, transmitted, displayed or otherwise published in any format, without the prior written permission of the copyright owner.

Disclaimer and Terms of Use: Provided that you maintain all copyright and other notices contained therein, you may download material (one machine readable copy and one print copy per page) for your personal and/or educational non-commercial use only.

The University of the Witwatersrand, Johannesburg, is not responsible for any errors or omissions and excludes any and all liability for any errors in or omissions from the information on the Library website.